Generalized path integral method for Elliott–Yafet spin relaxations in quantum wells and narrow wires

2012 J. Phys.: Condens. Matter 24 075801

(http://iopscience.iop.org/0953-8984/24/7/075801)

IOP PUBLISHING JOURNAL OF PHYSICS: CONDENSED MATTER

J. Phys.: Condens. Matter **24** (2012) 075801 (9pp) doi:10.1088/0953-8984/24/7/075801

Generalized path integral method for Elliott–Yafet spin relaxations in quantum wells and narrow wires

Jengjan Tsai and Cheng-Hung Chang

Institute of Physics, National Chiao Tung University, Hsinchu 300, Taiwan

E-mail: chchang@mail.nctu.edu.tw

Received 10 August 2011, in final form 27 November 2011
Published 18 January 2012
Online at stacks.iop.org/JPhysCM/24/075801

Abstract

We generalized the semiclassical path integral method originally used in the D'yakonov–Perel' mechanism to study the spin relaxation of the Elliott–Yafet mechanism in low-dimensional systems. In quantum wells, the spin properties calculated by this method confirmed the experimental results. In two-dimensional narrow wires, size and impurity effects on the Elliott–Yafet relaxation were predicted, including the wire-width-dependent relaxation time, the polarization evolution on the sample boundaries, and the relaxation behavior during the diffusive–ballistic transition. These properties were compared with those of the D'yakonov–Perel' relaxation calculated under similar conditions. For ballistic narrow wires, we derived an exact relation between the Elliott–Yafet relaxation time and the wire width, which confirmed the above simulations.

(Some figures may appear in colour only in the online journal)

1. Introduction

Spin relaxation is one of the central issues in the study of spintronics [1–3]. This phenomenon is ubiquitous in materials with spin polarization and has a long research history dating back to the Elliott–Yafet (EY) relaxation in simple metals (see [3] and recent papers citing this review). The study in this context is largely motivated by a fundamental interest in material properties. However, the pursuit of efficient spin manipulation in devices might further boost the progress in this field. Today, several types of mechanisms responsible for different spin relaxations have been found [4–7], and, among these, the D'yakonov–Perel' (DP) and EY mechanisms play essential roles. The former is due to spin precession between the momentum scattering events, while the latter occurs 'during' the momentum scattering events. These mechanisms affect the spin dynamics in various materials. For instance, in zinc-blende semiconductors at low temperatures, the spin relaxation is dominated by the DP mechanism [8–13]. In InGaAs/InP multiple quantum wells at room temperature [14, 15] and Te-doped InSb/$Al_{0.15}In_{0.85}Sb$ at low temperatures [16], the spin lifetime depends mainly on the EY mechanism [17–20]. In the past, a large number of experimental and theoretical studies have been devoted to the DP mechanism, either in the 3D bulk or in low-dimensional systems like quantum wells (QWs) and 2D narrow wires [13, 21–28]. However, comparatively less effort has been put into studying the EY relaxation, especially in low-dimensional systems [29]. In this work, we investigated the EY relaxation in QWs and 2D narrow wires in both the diffusive and the ballistic regimes.

The tool employed was the generalized semiclassical path integral (GSPI) method, which was extended from the original semiclassical path integral (SPI) approach for Rashba interaction [24, 25, 27]. The SPI approach has proved itself to be a powerful method for studying spin transport and spin relaxations in several mesoscopic systems [24, 25, 27]. It is one of many numerical approaches for understanding spin dynamics. Others include the microscopic approach [30], the Boltzmann equation approach [31], the two-component drift–diffusion approach [32], and Monte Carlo based techniques [33]. Despite all these approaches having been applied to the DP relaxation, they have rarely been used in the EY relaxation. The SPI and GSPI methods

arise from a similar concept to the Monte Carlo approach and are suitable for exploring spin problems in both diffusive and ballistic regimes bounded by arbitrary geometries.

In this work, we generalized the SPI approach from the DP to the EY relaxations. This generalized formalism was applied to real samples and gave results in accordance with the experimentally measured values [16]. Based on this consistency, we used this method to study the impurity and sample size effects on the EY relaxation under broad sample conditions. The main issues were how the relaxation time changed with sample width, how the polarization evolved on the boundary, and how the impurity density variation from the diffusive to the ballistic regimes affected the EY relaxation. Furthermore, the DP relaxation was calculated under the same sample conditions in order to compare it with the EY results. Finally, an analytical formula was derived for ballistic narrow wires, which confirmed our simulations and revealed exactly how the EY relaxation time varied with the wire width.

The paper is organized as follows. In section 2, the original SPI method is reformulated for systems with an EY mechanism. In section 3, the validity and precision of using the GSPI method on the experimental samples are examined and compared with the theoretical results. In sections 4 and 5, the effects of size and impurity, respectively, on the EY relaxation are studied by the GSPI method and compared with the DP relaxation. Finally, a summary and discussion are given in section 6.

2. The generalized semiclassical path integral formalism

The original SPI method was formulated for Rashba systems, and has the Hamiltonian

$$H = H_0 + H_{\mathrm{SOI}}, \tag{1}$$

where H_0 consists of the kinetic and potential energies of an electron in the system and H_{SOI} represents its spin–orbit interaction (SOI). Since the energy of spin–orbital coupling in the material of interest is usually much smaller than the kinetic and potential energies, the electron trajectory γ can be determined purely by H_0. The spin dynamics of this electron will be described by an evolution operator in the path integral formalism,

$$U_\gamma = \exp\left[-\frac{\mathrm{i}}{\hbar}\int_\gamma H_{\mathrm{SOI}}(t)\,\mathrm{d}t\right]. \tag{2}$$

If the electron collides with the impurities or boundaries n_γ times, its trajectory γ will comprise $n_\gamma + 1$ straight segments,

$$\gamma = \gamma_{n_\gamma+1} + \cdots + \gamma_2 + \gamma_1. \tag{3}$$

The corresponding spin evolution operator U_γ becomes a product

$$U_\gamma = U_{\gamma_{n_\gamma}} \times \cdots \times U_{\gamma_2} \times U_{\gamma_1} \tag{4}$$

of the individual operators $U_{\gamma_j} = \exp[-\frac{\mathrm{i}}{\hbar}H_{\mathrm{SOI}}t_{\gamma_j}]$, where t_{γ_j} is the time the electron spends to travel through the distance γ_j. These operators possess a time order property and do not commute with each other. This formalism can be easily extended to other systems governed by the DP mechanism, like the Dresselhaus Hamiltonian.

In systems under the EY mechanism, the Hamiltonian of the electron can be separated into two parts

$$H = H_0 + H_{\mathrm{int}}. \tag{5}$$

The unperturbed part

$$H_0 = \frac{\mathbf{p}^2}{2m} + V(\mathbf{r}) + \frac{\hbar}{4m^2c^2}(\nabla V(\mathbf{r}) \times \mathbf{p}) \cdot \boldsymbol{\sigma} \tag{6}$$

consists of, respectively, the kinetic energy, the periodic potential $V(\mathbf{r})$ of the lattice, and the spin–orbit interaction caused by $V(\mathbf{r})$ [17, 18]. Therein, m, $\mathbf{r}$, $\mathbf{p}$, and $\boldsymbol{\sigma}$ are the mass, position, momentum, and spin state of the electron, and c is the speed of light. The second part H_{int} in (5) is a perturbing Hamiltonian which contains several interactions responsible for the electron scattering. These scattering potentials could arise from impurities, heavy holes, phonons, piezo-acoustic modes, or boundaries, etc [17–19]. The EY relaxation discussed in the following can be ascribed to any of the above scattering potentials.

Without the SOI in (6), the wavefunctions of H_0 are the well-known Bloch functions

$$u_k \mathrm{e}^{\mathrm{i}\mathbf{k}\cdot\mathbf{r}}, \tag{7}$$

where u_k has the translational symmetry of the lattice. If the SOI term is present as in (6), the eigenfunctions of H_0 are a linear combination of two spin states [17],

$$(a_k|S_z;+\rangle + b_k|S_z;-\rangle)\,\mathrm{e}^{\mathrm{i}\mathbf{k}\cdot\mathbf{r}}, \tag{8}$$

where a_k and b_k are two functions with the same symmetry as $V(\mathbf{r})$ and u_k. The spin states $|S_z;+\rangle$ and $|S_z;-\rangle$ have angular momentum $\pm\frac{1}{2}\hbar$ along the $\mathbf{z}$ direction. Now, let us take H_{int} into account and consider a scattering, which changes the electron momentum from $\mathbf{k}$ to $\mathbf{k}'$. If the electron spin does not flip during this scattering, the electron momentum relaxation time τ_p is related to H_{int} by [17, 20]

$$\frac{1}{\tau_p} \propto \left|\int a^*_{k'} H_{\mathrm{int}} a_k \mathrm{e}^{\mathrm{i}(\mathbf{k}-\mathbf{k}')\cdot\mathbf{r}}\,\mathrm{d}\mathbf{r}\right|^2. \tag{9}$$

If the spin flips during the scattering, the spin relaxation time T_1, often called the longitudinal time or spin–lattice time [3], is given by [17, 20]

$$\frac{1}{2T_1} \propto \left|\int (a_{-k'} H_{\mathrm{int}} b_k - b_{-k'} H_{\mathrm{int}} a_k)\mathrm{e}^{\mathrm{i}(\mathbf{k}-\boldsymbol{k}')\cdot\mathbf{r}}\,\mathrm{d}\mathbf{r}\right|^2, \tag{10}$$

which has around the same proportionality constant as (9). When the electron encounters a scattering at ξ, whether its spin state flips or not will be determined by the stochastic operator (in $SU(2)$ representation)

$$U_\xi = \begin{cases} \begin{pmatrix} 0 & 1 \\ 1 & 0 \end{pmatrix} := I_{\mathrm{flip}}, & \text{flip probability } \phi, \\ \begin{pmatrix} 1 & 0 \\ 0 & 1 \end{pmatrix} := I_{\mathrm{unflip}}, & \text{non-flip probability } 1-\phi, \end{cases} \tag{11}$$

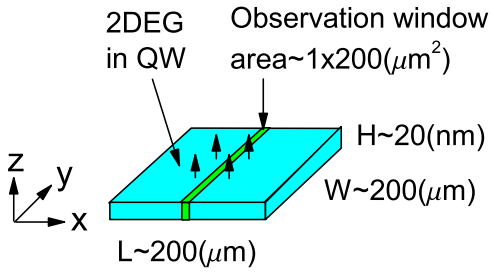

Figure 1. A quasi-2D sample and an observation window which is a stripe of area $1 \times 200\ \mu\text{m}^2$. For a quantum well with large L and W, the stripe is long and the average spin behavior therein is almost the same as that in the whole well (for the cases in figures 2 and 3). For a narrow wire with large L but small W, the stripe is short and the average spin behavior inside it is a local spin dynamics along the wire (for the case in figure 7).

where $0 \leq \phi \leq 1$. To realize this process in a simulation, one can randomly take a number x between 0 and 1 at a scattering. Then the operator

$$U_\xi = \Theta(\phi - x) I_{\text{flip}} + \Theta(x - \phi) I_{\text{unflip}} \tag{12}$$

will decide stochastically whether the spin will flip, where Θ is the Heaviside function. The flip probability is related to the flip frequencies in equations (9) and (10) by

$$\frac{\frac{1}{\tau_p}}{\frac{1}{2T_1}} = \frac{1-\phi}{\phi}, \qquad \text{or} \qquad \phi = \frac{\tau_p}{2T_1 + \tau_p}. \tag{13}$$

This probability ϕ can be calculated from T_1 and τ_p, provided they can be measured experimentally.

If an electron encounters scattering n_γ times at points ξ_1, ξ_2,..., ξ_{n_γ}, the corresponding spin evolution operator U_γ will be

$$U_\gamma = U_{\xi_{n_\gamma}} \times \cdots \times U_{\xi_2} \times U_{\xi_1}. \tag{14}$$

This formula for the EY mechanism resembles (4) for the Rashba systems. However, U_γ in (14) flips the spin only at discrete times when a scattering occurs, whereas that in (4) changes the spin at any time. With the microscopic information on each individual spin from (14), any macroscopic average of a crowd of spins can be calculated. Suppose the 2D sample is put on the **xy**-plane, as shown in figure 1. The main quantity of interest in the following is the spin polarization in the **z**-direction,

$$P_z(t) = \frac{1}{n_{(t,D)}} \sum_{\text{electrons at } (t,D)} s_z(t), \tag{15}$$

which averages over the **z** component of the spin states $s_z(t)$ of all $n_{(t,D)}$ electrons in an observation window D at time t. When the spin of an electron is polarized to the **z** direction, s_z is set to 1. Therefore, the maximum value of $|P_z(t)|$ is 1, which corresponds to all electrons being aligned in the **z** direction.

To apply the GSPI method in a simulation, a large number of electrons are initially uniformly distributed in the sample. All electrons are polarized in the **z** direction and run isotropically with the Fermi velocity v_F. In the following, this condition is referred to as the standard initial condition.

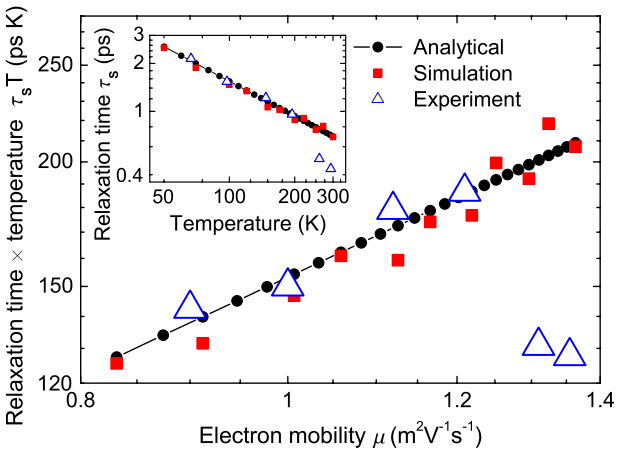

Figure 2. A comparison between the analytical, numerical, and experimental relations between $\tau_s T$ and mobility μ, as well as between τ_s and temperature T (inset). The large triangle size indicates the experimental error bar.

Each electron moves in a straight line before a scattering. The distance γ_j between two scatterings conforms to the well-known exponential free path distribution, which can be derived as in the Beer–Lambert law. In the simulation, γ_j is obtained from $\gamma_j = -l_{\text{mfp}} \cdot \ln(x)$, where l_{mfp} is the mean free path and x is a stochastic number between 0 and 1. We assume that the wires have smooth boundaries on which the electron reflection is specular. For samples with rough boundaries, one should modify the reflection angles according to the microscopic details.

3. The GSPI approach for experimental samples

The spin relaxation caused by the EY mechanism has been explored by some experimental groups [14–16]. In [16], the sample is an InSb/$Al_{0.15}In_{0.85}Sb$ single QW grown by MBE on a GaAs substrate. The QW has a well width of 20 nm (corresponding to the height in figure 1) and is uniformly Te-doped (sample number me1831F). The electron densities in this sample are 5.7×10^{11} cm^{-2} at 77 K and 7.3×10^{11} cm^{-2} at 300 K. Since the carrier concentration of a semiconductor is proportional to T [34], the concentration for other T values between these values can be linearly interpolated, as $n_e(T) \approx (0.0072T + 5.15) \times 10^{10}$ cm^{-2}. The mobility of this sample was measured by means of the Hall effect and behaved as $\log_{10}\mu(T) \approx 0.28 \times \log_{10}T - 0.55$ m^2 V^{-1} s^{-1} within $T =$ 50–300 K. For more temperature dependent factors in spin relaxations, the reader is referred to [23].

Figure 2 shows the product of the spin relaxation time with the temperature, $\tau_s T$, versus the carrier mobility μ. Its inset depicts the spin relaxation time versus the temperature of the sample. In both plots, the triangles are the experimental data measured from the sample me1831F, which is mainly governed by the EY mechanism. The black dots are calculated from the formula [16]

$$\frac{1}{\tau_s} = C_{\text{EY}} \eta^2 \left(1 - \frac{m^*}{m}\right)^2 \frac{E_{1e}}{E_g^2} kT \frac{1}{\tau_p}. \tag{16}$$

Therein, m is the real electron mass, m^* denotes the effective mass in the conduction band, E_g represents the band gap, E_{1e} stands for the confinement energy of the lowest electron subband, τ_s is the EY mechanism induced spin relaxation time which is equal to T_1 in equation (10), and $\eta = \Delta/(E_g + \Delta)$ with the spin–orbit splitting energy Δ. The momentum relaxation time τ_p is related to the mobility μ by $\tau_p = \mu m^*/e$ and the dimensionless constant C_{EY} is believed to be of the order of unity. The black dots in figure 2 are calculated from (16) by using the following parameters of me1831F: $\Delta \approx 0.81$ eV, $E_g \approx 0.24$ eV, $m^*/m \approx 0.014$, $E_{1e} \approx 0.08$ eV and $C_{EY} \approx 7.5$ [16]. Recall that τ_s can be affected by various scattering potentials mentioned below (6). Among others, phonons will become more significant at high T.

Figure 2 shows that both the experimental and theoretical studies give the relation $\tau_s T \propto \mu$ for most μ. But two experimental points have an opposite trend $\tau_s T \propto \mu^{-1}$ at high μ, which corresponds to the high T regime in the sample me1831F, as known from the empirical $\mu(T)$ relation mentioned at the beginning of this section. It is believed that this opposite trend is because the DP mechanism overrides the EY mechanism in the high μ regime, according to the current understanding that $\tau_s T \propto \mu$ for the EY mechanism and $\tau_s T \propto \mu^{-1}$ for the DP mechanism [16]. The latter is supported by the observation on the sample me1833 (remotely n-doped with Te 20 nm above the well) in [16], which follows the DP mechanism and has the property $\tau_s T \propto \mu^{-1}$.

Next, the relaxation properties will be calculated by the GSPI simulation. To compare with the above experimental results, the following experimental parameters need to be inserted in the simulations. First, the spin flip probability ϕ will be calculated by (13), where the way in which $\tau_p = \mu m^*/e$ and T_1 vary with T is based on the above empirical relation $\mu(T)$ and the black dots in the inset of figure 2, which are calculated from (16). Second, v_F can be derived from $v_F = \hbar/m^*\sqrt{2\pi n_e}$ with the above empirical electron density $n_e(T)$. Notice that since n_e lies between 5.5×10^{11} and 7.3×10^{11} cm^{-2}, the corresponding de Broglie wavelength $\lambda_F = \sqrt{2\pi/n_e}$ ranging from 34 to 30 nm is larger than the sample height of 20 nm, as shown in figure 1. Thus, the electrons are confined in the **z** direction of the sample. Third, the size of the experimental sample was not explicitly mentioned in [16]. However, (16) therein is referred to [14, 15], where the sample sizes are about 2 in (approximately 5×10^4 μm) in length. Our simulation is performed on a smaller square of 2×10^2 μm in length for less consumption of computational resources. Both the experimental and the simulation samples belong to bulk systems. Since their scales are much larger than the de Broglie wavelength λ_F (30–34 nm), the electron motion on the **xy** plane is more particle-like and the validity of the semiclassical GSPI approach is justified. We put 4×10^6 electrons into our 2D sample, which are initially in the standard initial condition and follow the simulation protocols at 50–300 K in table 1. The time course of the polarization $P_z(t)$ is recorded in the middle of the sample (figure 1).

The observed $P_z(t)$ is an exponential function with a relaxation time τ_s. During the temperature variation in table 1, the relations $(\tau_s T, \mu)$ and (τ_s, T) can be calculated, and are plotted as red squares in the main plot and the inset of figure 2, respectively. Notice that our recent theoretical study and simulation reveal that the $P_z(t)$ of the DP relaxation in a narrow wire will transit from an exponential function to a Bessel function during the impurity density decline [27]. Such $P_z(t)$ deviation from an exponential function will not occur in the EY mechanism, as we shall prove in section 5. Thus, here we can characterize $P_z(t)$ properly by the parameter τ_s without worrying about its deformation.

The red squares in figure 2 calculated by the GSPI method show very close agreement with the theoretical and experimental results for most μ, with the same relation $\tau_s T \propto \mu$. The opposite experimental trend $\tau_s T \propto \mu^{-1}$ in the high μ regime is not seen in our simulation. This indirectly supports the previous hypothesis that $\tau_s T \propto \mu^{-1}$ arises from other mechanisms, because the pure EY mechanism in our GSPI simulation cannot produce this trend. The main plot of figure 2 does not explicitly tell us how τ_s varies with T. In fact, T can influence the sample me1831F in two ways. First, a large T will increase the electron mobility μ and subsequently $\tau_p = \mu m^*/e$, which in turn will reduce the electron scattering per unit traveling distance. However, a large T also will enhance the spin flip probability ϕ (see table 1) and make the spin flip more frequently. When the two effects blend together, it is hard to predict how τ_s will change with T. Nevertheless, an obvious τ_s decay is readily seen, when we transform the $(\tau_s T, \mu)$ data into the (τ_s, T) plot in the inset.

4. The size effect on the EY relaxation

The size effect on the spin relaxation is another interesting issue in spintronics. For instance, the group of Awschalom has carried out some measurements on the DP relaxation in narrow wires of different widths [26]. However, to the best of our knowledge, very few experiments have investigated the size effect on the EY relaxation. A study close to this topic was the EY relaxation in granular systems [29], but the sample size there was fixed. In this section, we will study how the EY spin relaxation changes with the width of a wire. Our sample has a length of 200 μm, while its width varies between 0.1 μm (narrow wire) and 200 μm (2D quantum well). We take 8×10^5 electrons in the standard initial condition and use the parameter values from table 1 for the simulations as before.

Figure 3 depicts the relaxation time τ_s versus the sample width W at various temperatures T. Three conclusions can be drawn from this plot.

(1) τ_s decreases with T.
(2) τ_s is nearly a constant for $W > 1$ μm at all T.
(3) τ_s drops abruptly to zero when $W < 1$ μm.

Phenomenon (1) has the same reasoning as that at the end of section 3. To account for phenomena (2) and (3), recall that for $W > 1$ μm the sample is like a bulk system. The electron spins in this system are flipped mainly by the impurities in the bulk and less by the sample boundaries. Therefore, the relaxation time τ_s is almost fully determined by the impurity

Table 1. The simulation protocols. T_1 is calculated by (16), $\tau_p = \mu m^*/e$, $v_F = (\hbar/m^*)\sqrt{2\pi n_e}$, $l_{mfp} = v_F\tau_p$, and ϕ is calculated by (13).

T (K)	50	70	100	120	150	170	200	220	250	270	300
T_1 (ps)	2.549 00	1.997 90	1.543 20	1.352 30	1.150 60	1.050 90	0.934 24	0.871 94	0.794 86	0.751 78	0.696 56
τ_p (ps)	0.066 19	0.072 63	0.080 14	0.084 28	0.089 63	0.092 78	0.097 03	0.099 62	0.103 20	0.105 41	0.108 52
v_F (μm ps^{-1})	1.5381	1.558 0	1.5874	1.606 7	1.635 3	1.654 0	1.681 7	1.700 0	1.727 0	1.744 7	1.771 0
l_{mfp} (μm)	0.101 80	0.113 16	0.127 22	0.135 41	0.146 56	0.153 45	0.163 18	0.169 35	0.178 21	0.183 91	0.19219
ϕ	0.012 82	0.017 85	0.025 31	0.030 22	0.037 49	0.042 28	0.049 37	0.054 04	0.060 96	0.065 51	0.072 27

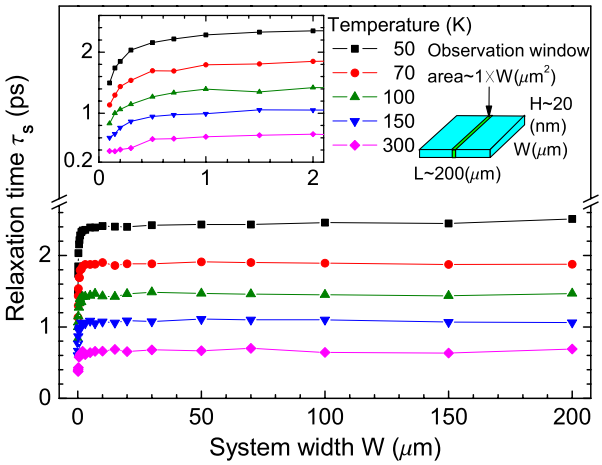

Figure 3. The EY spin relaxation time versus the wire width at five different temperatures, observed on a stripe of area $1 \times W$ μm^2. The inset is magnified from the main plot.

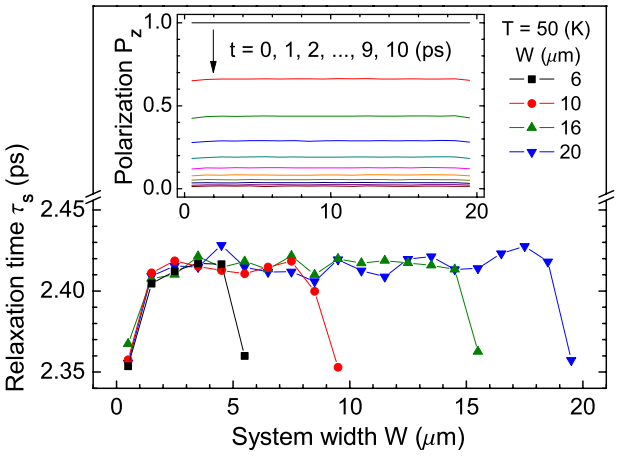

Figure 4. The EY spin relaxation time versus four wire widths at 50 K, observed on a square of area 1×1 μm^2 scanning along the wire width in the middle of the sample. The inset is the evolution of spin polarization along the width $W = 20$ μm.

density and is thus a constant of W. However, for $W < 1$ μm, the boundary induced spin flip becomes more significant. The smaller the sample width is, the higher the collision frequency will be, and the faster the spin will flip. When W approaches zero, τ_s tends to zero, because almost all the electrons collide with the boundaries infinitely often, except the minority of electrons moving exactly along the wire axis.

It is well known that the DP relaxation near the sample boundary behaves differently from that far from the boundary [27, 35, 36]. An interesting question is whether the EY relaxation will behave similarly on the boundary. To answer this question, we shrink the observation window to a small square of area 1×1 μm^2 and use this window to scan the local τ_s at different positions along the width direction of a wire. Figure 4 depicts the EY relaxation time τ_s, which remains close to a constant inside the sample, until the drops near the two boundaries. How close to the boundaries τ_s will begin to drop is an open question requiring further study. Moreover, the inset of figure 4 shows that $P_z(t)$ is almost flat until the slight drops on the boundaries. These drops will become apparent, if we magnify the individual $P_z(t)$ curves.

For a comparison, we calculate the τ_s of the DP relaxations along a wire of width 6–50 μm, as shown in figure 5. The initial electron and spin states in the simulation are the same as in the above EY cases, while the temperature is as low as 5 K to mimic the real experimental environment. The corresponding Fermi velocity and mean free path are $v_F = 0.37$ μm ps^{-1} and $l_{mfp} = 0.28$ μm and the spin rotation length (as defined in [24, 25, 27]) is $L_{so} = 2$ μm. The

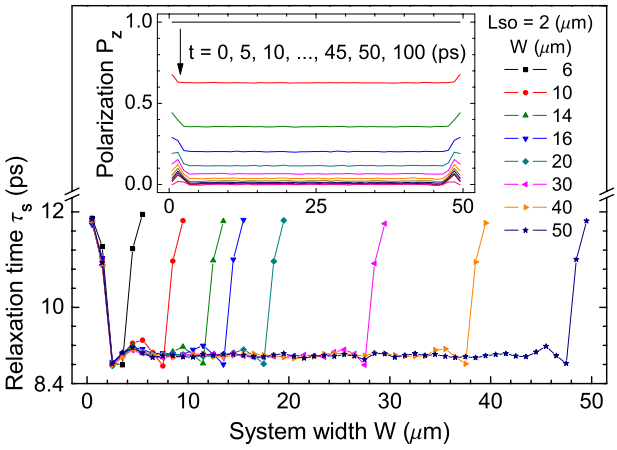

Figure 5. The DP spin relaxation time versus eight wire widths at $T = 5$ K and $L_{so} = 2$ μm, observed on a square of area 1×1 μm^2 scanning along the wire width in the middle of the simulation sample. The inset is the evolution of spin polarization along the width $W = 50$ μm.

simulation method is as referred to in [27]. In contrast to the EY relaxation, the DP relaxation time near the boundary is larger than that elsewhere (figure 5). Moreover, the $P_z(t)$ of the DP relaxation on the boundary exhibits a hump structure (inset of figure 5), which is opposite to the EY relaxation and is a main difference between these two relaxations. The τ_s increase on the boundary in the DP relaxation is ascribed to the reverse rotation of spins [27, 36], whereas the τ_s decrease

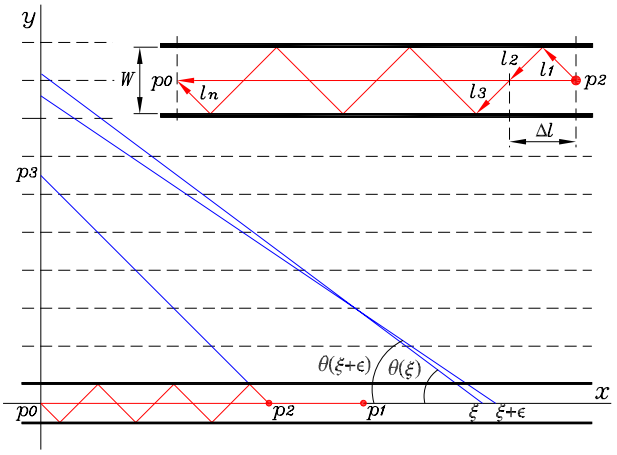

Figure 6. In a ballistic narrow wire, a straight trajectory $\overline{p_1p_0}$ and a zigzag trajectory $\widetilde{p_2p_0}$ have the same length $l = v_F t$. The length of $\widetilde{p_2p_0}$ is equal to that of $\overline{p_2p_3}$, since the former can be regarded as a multiple mirror reflection of the latter with respect to the horizontal dashed lines. The values $\theta(\xi)$ and $\theta(\xi+\epsilon)$ are the outgoing angles of the electrons at ξ and $\xi+\epsilon$, respectively, along which the electrons can reach p_0 after running through the same distance l. The inset is a magnification of $\widetilde{p_2p_0}$.

on the boundary in the EY relaxation is due to more frequent boundary collisions.

5. The impurity effect on the EY relaxation

When the mean free path of the electrons exceeds the wire width, the system will enter the ballistic regime. The $P_z(t)$ of the DP relaxation undergoes a drastic change from an exponential function to a Bessel function during the diffusive–ballistic transition [27]. In this section, we will examine how the $P_z(t)$ of the EY relaxation behaves in the ballistic regime.

Suppose an ensemble of electrons in the standard initial conditions are placed in a narrow wire as in figure 6. The spin polarization $P_z(t)$ observed at the origin p_0 at time t is averaged from the spin states of all electrons which arrive at p_0 at time t. These electrons can arrive through a straight trajectory or various zigzag ones, like $\overline{p_1p_0}$ and $\widetilde{p_2p_0}$ in figure 6, all of which have the same length $l = v_F t$. Depending on the trajectory types, these electrons will launch at different x values at time 0. Suppose $\tilde{s}_z(x)$ is the **z** component of the spin state of an electron at p_0 at time t when it starts at x at time 0. Then $P_z(t)$ is an average over all these spin states [27],

$$P_z(t) = \frac{\int_{-l}^{l} \tilde{s}_z(x)\rho w(x) W \,\mathrm{d}x}{\int_{-l}^{l} \rho w(x) W \,\mathrm{d}x}, \tag{17}$$

where $w(x)$ is a weight proportional to the number of electrons starting at x and contributing to $\tilde{s}_z(x)$ and ρ denotes the constant surface density of the electrons in the wire. Notice that since the spin flip in the EY mechanism is a stochastic process, two electrons, even when running along the same trajectory, may have different final spin states. Thus, the spin state $\tilde{s}_z(x)$ should be understood as an ensemble average taken from all electrons running along the same trajectory. The fluctuation around this average is extremely small for real materials having the typical electron density 10^{11} cm^{-2}. If an electron starting between x and $x+\varepsilon$ (for the case $x \geq 0$) has to arrive at p_0 at time t, its initial outgoing angle must lie between $\theta(x)$ and $\theta(x+\varepsilon)$, with $\varepsilon \ll 1$ (see the example for $x = \xi$ in figure 6). Thus, the weight $w(x)$ becomes the fraction of electrons at x running within these two angles over those within the whole 2π angle. If the electrons are uniformly distributed in the wire with isotropic outgoing angles, the fraction of electron number equals the fraction of orientation range [27],

$$\begin{aligned} w(x) &= \frac{1}{2\pi} 2\left[\theta(x) - \theta(x+\varepsilon)\right] \\ &= \frac{1}{\pi}\left[\arccos\left(\frac{x}{l}\right) - \arccos\left(\frac{x+\varepsilon}{l}\right)\right], \end{aligned} \tag{18}$$

where the factor 2 arises from the two mirror-symmetric orientations $\pm\theta$.

While the fraction $w(x)$ for EY relaxation is similar to that for DP relaxation, $\tilde{s}_z(x)$ is completely different for the two relaxations. To obtain $\tilde{s}_z(x)$ of the EY mechanism, we need to know how many scatterings an electron running from x to p_0 will encounter and how its spin state will be changed by these scatterings. If an electron is initially polarized in the **z** direction and encounters scattering n times, its **z** component of the spin state will on average change to the value (see (A.6) in the appendix)

$$\bar{s}_z(n) = \exp\left(-\frac{n}{\tau}\right), \qquad \text{with } \tau = \frac{1-\phi}{2\phi}, \tag{19}$$

where ϕ is the spin flip probability in (13). Note that $s_z(t)$, $\tilde{s}_z(x)$, and $\bar{s}_z(n)$ in equations (15), (17), and (19) describe the spin state as a function of t, x, and n, respectively. If an electron at p_2 in figure 6 has the outgoing angle $\theta(p_2)$ and travels a distance $l = v_F t$ along a zigzag trajectory to arrive at p_0 at time t, it will collide with the two boundaries n times with

$$n \approx \frac{x}{\Delta l} = \frac{x}{W\cot\theta(p_2)} = \frac{\sqrt{l^2 - x^2}}{W}, \tag{20}$$

where Δl is the distance between two collisions projected on the **x** axis (inset of figure 6). Inserting (20) into (19), $\bar{s}_z(n)$ becomes a function of x,

$$\tilde{s}_z(x) = \exp\left[-\left(\frac{\sqrt{l^2 - x^2}}{W}\right)\frac{1}{\tau}\right]. \tag{21}$$

Inserting (18) and (21) into (17), the evolution of $P_z(t)$ at the observation point p_0 will become completely known. Although this formula is too complicated to have a closed form, its value can be evaluated numerically.

To test the accuracy of (17), let us consider three wires of widths $W = 0.01$, 0.02, and 0.04 μm with the parameter values for 50 K in table 1 and record $P_z(t)$ in the middle of the wires. In the main plot of figure 7, the black squares, red circles, and blue triangles come from simulations, while the black dotted, red dotted–dashed, and blue dashed curves are calculated by (17). The two sets of data agree very well

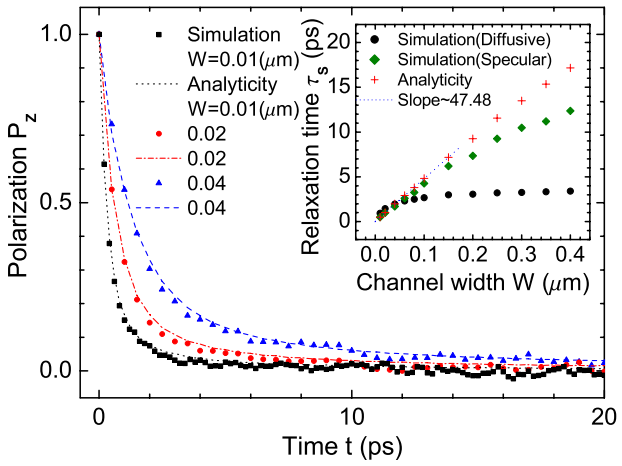

Figure 7. The polarization $P_z(t)$ versus the time t in three wires of different widths. The square, circle, and triangle symbols denote the simulation data and the different lines are calculated by the formula (17). The inset shows the spin relaxation time versus the wire width from simulations (green rhombuses) and the analytical approach (17) (red crosses), fitted by a straight line (blue dotted). These are all results of (17) for specular boundary reflections. For diffusive reflections, the (τ_s, W) relation is plotted by the black circles in the inset.

with each other. They behave like exponential functions with the relaxation times plotted in the inset of figure 7. In this simulation, we narrowed W down to 10 nm. This value is smaller than the height $H = 20$ nm of the experimental sample and has reached the quantum regime in the width direction, since the Fermi wavelength at 50 K is about 30 nm for semiconductors. We took this extreme W in the simulation to verify whether (17) was mathematically correctly derived. The reader should not be puzzled by the physical validity of the semiclassical approach. For samples with $W = 0.2$ μm, this formula still predicts a rather close value to the simulated relaxation time (see the inset in figure 7).

Figure 7 also indicates that in a ballistic wire the DP and EY relaxation times vary rather differently with the wire width W. When $W \to 0$, the $P_z(t)$ of the DP relaxation will converge to a Bessel function [27], but that of the EY relaxation (main plot of figure 7) remains as an exponential function, whose relaxation time decreases with vanishing W. That is, at $W \approx 0$, the DP relaxation is insensitive to W, but the EY relaxation is sensitive to W. The reason is that in the limit $W \to 0$, most electrons are confined in the width direction and collide with the boundaries at very high frequencies. The spins of these electrons tend to be frozen (in the width direction) in the DP mechanism, due to the motional narrowing effect [35], but will be accelerated to flip in the EY mechanism, due to the increasing collision frequency. This leads to the drastic distinction between the $P_z(t)$ of the DP and EY mechanisms in the ballistic narrow wires.

In the inset of figure 7, the τ_s obtained from (17) begin to deviate from those of the GSPI simulation at $W \approx 0.1$ μm. This W is five times larger than the sample height in [16]. Beyond this W, higher order corrections in equations (18) and (21) are required to improve the accuracy of (17). For $W \to 0$, both simulation and the exact formula give the same ratio $\tau_s/W \approx 47.48$. To account for this value, notice that the denominator of (17) is independent of l and t. The function $\tilde{s}_z(x)$ in the numerator varies slowly for most $x \in [-l, l]$, but increases sharply with $|x|$ in the two small regions $[-l, -l+\varepsilon']$ and $[l - \varepsilon', l]$, with the limit $\tilde{s}_z(\pm l) = 1$. In contrast, $w(x)$ increases comparatively moderately within $[-l, l]$, with the limit $w(l - \varepsilon') = \arccos(1 - \varepsilon'/l)/\pi \approx (\sqrt{2\varepsilon'/l})/\pi$. Thus, $w(x)$ can be approximately regarded as a constant C and taken out of the integral in the numerator of (17). Dropping all l-independent terms, one obtains the proportional relation

$$P_z(t) \propto C \int_{-l}^{l} \tilde{s}_z(x)\,\mathrm{d}x \propto \int_{l-\varepsilon'}^{l} \tilde{s}_z(x)\,\mathrm{d}x \approx \tilde{s}_z(x)\varepsilon'\big|_{x\approx l}. \quad (22)$$

Using a Taylor expansion in (21), it yields a rough estimation

$$P_z(t) \propto \exp\left[-\frac{l}{\tau W}\left(1 - \frac{1}{2}\left(\frac{x}{l}\right)^2 - \cdots\right)\right]_{x\approx l}$$
$$\approx \exp\left(\frac{-v_F t}{2\tau W}\right) \equiv \exp\left(\frac{-t}{\tau'}\right), \quad (23)$$

where $\tau' = 2\tau W/v_F$, which, together with (19), gives the ratio $\tau'/W = (\frac{1}{\phi} - 1)/v_F \approx 50.08$. This ratio is very close to the 47.48 obtained from the simulation (inset of figure 7), even though we only consider a small part of the integral around $x \approx \pm l$ in equation (17). Physically, it highlights the essential contribution of the electrons starting at $x \approx \pm l$. These electrons run almost along the wire axis and are nearly free from collisions with the boundaries. They have no spin flip within time t and will give the main contribution to the non-zero value of $P_z(t)$ at t.

The $P_z(t)$ discussed above comes from the expression (17), which is based on the assumption of specular reflections on the boundary. For diffusive reflections, a large number of new trajectories will contribute to $P_z(t)$, in addition to the old ones in (17). Along the wire direction, an old trajectory can only have unidirectional movement, while a new trajectory usually contains both forward and backward motions, similar to the trajectories of a random walker. Given an initial point p_2, a final point p_0, and a fixed time t, there exists only one old trajectory (figure 6); however, a bunch of new trajectories are allowed under the same conditions. The shorter the distance $\overline{p_2p_0}$ is, the more allowed new trajectories can be found, just like a random walker has more possible routes to reach a point closer to its initial position. Since the trajectories of shorter $\overline{p_2p_0}$ have more boundary collisions under a fixed t, $P_z(t)$ for diffusive reflections contains on average more trajectories of high reflection frequencies than $P_z(t)$ for specular reflections. Thus, intuitively one would expect a faster polarization relaxation for diffusive reflections, which is generally true, as confirmed by the simulations depicted by the black circles in the inset of figure 7. However, since the relaxation times of all reflections decrease with wire width, the τ_s difference between specular and diffusive reflections becomes insignificant for extremely narrow wires.

6. Conclusion

In this work, we generalized the semiclassical path integral method and extended its application to systems governed by the EY relaxation mechanism. The spin relaxation times

calculated by this method are in accordance with the values measured in experiments (figure 2). For the size effect, the EY relaxation time τ_s remains nearly constant for large wire width, but drops abruptly to zero if W shrinks to a certain extent (figure 3). This trend is robust against various temperatures, electron mobilities, and electron densities. Near the geometric boundaries, the local τ_s falls rapidly (figure 4), because the boundaries enhance the scattering frequency and the spin relaxation speed, in contrast to that in the DP relaxation. The τ_s and relaxation patterns of both the EY and the DP mechanisms were calculated and compared (figures 4 and 5). For ballistic narrow wires, we derived an analytical formula (17) for the EY spin relaxation, which confirms the above simulated $P_z(t)$ (figure 7). This formula explicitly relates the EY spin relaxation time τ_s to the wire width. The predicted τ_s is in good agreement with the simulated value (inset of figure 7).

The above results were calculated based on two assumptions. First, all electrons contributing to the polarization were on the Fermi surface. In reality, the electron velocity may deviate from this unique value. However, our tests on various velocity distributions showed that the spin relaxation behaviors, especially the relation $\tau_s T \propto \mu$, were less sensitive to this factor. Thus, we presented the simplest distribution concentrated at the Fermi velocity. Second, the scattering rates on the boundary and impurities were assumed to be the same. This was due to the lack of microscopic details on each individual scattering. Although this assumption may not be true for general materials, it does not affect our comparison with the experimental results on the quantum wells, because these wells are so large that the details of boundary scattering are insignificant. For ballistic narrow wires, the boundary scattering becomes important and the results presented here are only a special example. Once the boundary reflection properties for other systems are known, extension of the spin relaxation study to these systems is straightforward.

Acknowledgments

We would like to acknowledge Roland Winkler and Chon-Saar Chu for helpful discussions as well as Anatoly G Mal'shukov for his inspiration on the SPI approach. This work is supported by the National Science Council in Taiwan through Grant No. NSC 97-2112-M-009-008-MY3.

Appendix

As discussed in the text before equation (18), the spin state in the EY mechanism should be understood as an ensemble average, since the spin flip in this mechanism is a stochastic process. Let $S_\uparrow(n)$ and $S_\downarrow(n)$ be the probabilities of a spin being in up and down states, respectively, after its electron encounters scattering n times. Clearly,

$$S_\uparrow(n) + S_\downarrow(n) = 1. \tag{A.1}$$

Under the EY mechanism, we have

$$\begin{aligned} S_\uparrow(n+1) &= (1-\phi)S_\uparrow(n) + \phi S_\downarrow(n) \\ &= S_\uparrow(n)(1-2\phi) + \phi, \end{aligned} \tag{A.2}$$

with the spin flip probability ϕ for each scattering, where (A.1) has been used. After scattering n and $n+1$ times, the average spin states in the **z** component are respectively

$$\begin{aligned} \bar{s}_z(n) &= S_\uparrow(n) - S_\downarrow(n) = 2S_\uparrow(n) - 1 \\ \bar{s}_z(n+1) &= 2S_\uparrow(n+1) - 1. \end{aligned} \tag{A.3}$$

Thus, the relation

$$\frac{\Delta \bar{s}_z(n)}{\Delta n} = \frac{\bar{s}_z(n+1) - \bar{s}_z(n)}{(n+1) - n} = -\frac{1}{\tau}\frac{\bar{s}_z(n+1) + \bar{s}_z(n)}{2} \tag{A.4}$$

is yielded, with $\tau = (1-\phi)/(2\phi)$. In the continuous limit, this yields

$$\frac{\mathrm{d}\bar{s}_z}{\mathrm{d}n} = -\frac{1}{\tau}\bar{s}_z. \tag{A.5}$$

According to this equation, if an electron is initially polarized in the **z** direction, i.e., $\bar{s}_z(0) = 1$, the **z**-component of this spin will evolve to

$$\bar{s}_z(n) = \exp\left(-\frac{n}{\tau}\right), \tag{A.6}$$

after scattering n times.

Alternatively, (A.6) can be obtained in a different way. Suppose we have an ensemble of electrons initially under standard conditions in a diffusive bulk sample, with the momentum relaxation time τ_p. If the average **z**-component of the spin state, $s_z(t)$, undergoes a longitudinal spin relaxation, it will decay exponentially, with the same relaxation time T_1 as that in (13),

$$s_z(t) = \exp\left(-\frac{t}{T_1}\right) \approx \exp\left(-\frac{n}{\tau^*}\right), \tag{A.7}$$

where $\tau^* = (1-\phi)/(2\phi)$, because $t \approx n\tau_p$ for n collisions within time t and $\tau_p/T_1 = (2\phi)/(1-\phi)$ according to (13). A comparison shows that τ in (A.6) and τ^* in (A.7) are exactly the same.

References

[1] Datta S and Das B 1990 *Appl. Phys. Lett.* **56** 665
[2] Wolf S A, Awschalom D D, Buhrman R A, Daughton J M, von Molnár S, Roukes M L, Chtchelkanova A Y and Treger D M 2001 *Science* **294** 1488
[3] Žutić I, Fabian J and and Das Sarma S 2004 *Rev. Mod. Phys.* **76** 323
[4] Ivchenko E L and Pikus G E 1997 *Superlattices and Other Heterostructures: Symmetry and Optical Phenomena* (Berlin: Springer)
[5] Song P H and Kim K W 2002 *Phys. Rev.* B **66** 035207
[6] Winkler R 2003 *Spin–Orbit Coupling Effects in Two-Dimensional Electron and Hole System* (Berlin: Springer)
[7] Fabian J and Das Sarma S 1999 *J. Vac. Sci. Technol.* B **17** 1708
[8] Dresselhause G 1955 *Phys. Rev.* **100** 580
[9] D'yakonov M I and Perel' V I 1971 *Sov. Phys.—JETP* **33** 1053
[10] D'yakonov M I and Perel' V I 1972 *Sov. Phys. Solid State* **13** 3023
[11] Bychkov Y A and Rashba E I 1984 *J. Phys. C: Solid State Phys.* **17** 6039
[12] D'yakonov M I and Kachorovskii V Yu 1986 *Sov. Phys. Semicond.* **20** 110

[13] Nitta J, Akazaki T, Takayanagi H and Enoki T 1997 *Phys. Rev. Lett.* **78** 1335
[14] Tackeuchi A, Kuroda T, Muto S, Nishikawa Y and Wada O 1999 *Japan. J. Appl. Phys.* **38** 4680
[15] Tackeuchi A, Kuroda T, Muto S and Wada O 1999 *Physica* B **272** 318
[16] Litvinenko K L, Murdin B N, Allam J, Pidgeon C R, Bird M, Morris K, Branford W, Clowes S K, Cohen L F, Ashley T and Buckle L 2006 *New J. Phys.* **8** 49
[17] Elliott R J 1954 *Phys. Rev.* **96** 266
[18] Zawadzki W and Szymańska W 1971 *Phys. Status Solidi* b **45** 415
[19] Fishman G and Lampel G 1977 *Phys. Rev.* B **16** 820
[20] Beuneu F and Monod P 1978 *Phys. Rev.* B **18** 2422
[21] Kiselev A A and Kim K W 2000 *Phys. Rev.* B **61** 13115
[22] Mal'shukov A G, Shlyapin V V and Chao K A 2002 *Phys. Rev.* B **66** 081311(R)
[23] Kainz J, Rössler U and Winkler R 2004 *Phys. Rev.* B **70** 195322
[24] Chang C-H, Mal'shukov A G and Chao K A 2004 *Phys. Lett.* A **326** 436
[25] Chang C-H, Mal'shukov A G and Chao K A 2004 *Phys. Rev.* B **70** 245309
[26] Holleitner A W, Sih V, Myers R C, Gossard A C and Awschalom D D 2006 *Phys. Rev. Lett.* **97** 036805
[27] Chang C-H, Tsai J, Lo H-F and Mal'shukov A G 2009 *Phys. Rev.* B **79** 125310
[28] Frolov S M, Lüscher S, Yu W, Ren Y, Folk J A and Wegscheider W 2009 *Nature* **458** 868
[29] Anaya A, Bowman M and Davidović D 2004 *Phys. Rev. Lett.* **93** 246604
[30] Mal'shukov A G and Chao K A 2000 *Phys. Rev.* B **61** 2413
Puller V I, Mourokh L G, Horing N J M and Smimov A Y 2003 *Phys. Rev.* B **67** 155309
Mishchenko E G and Halperin B I 2003 *Phys. Rev.* B **68** 045317
[31] Fabian J and Das Sarma S 2002 *Phys. Rev.* B **66** 024436
Qi Y and Zhang S 2003 *Phys. Rev.* B **67** 052407
Schliemann J and Loss D 2003 *Phys. Rev.* B **68** 165311
[32] Yu Z G and Flatté M E 2002 *Phys. Rev.* B **66** 201202
Martin I 2003 *Phys. Rev.* B **67** 014421
Pershin Y V and Privman V 2003 *Phys. Rev. Lett.* **90** 256602
[33] Kiselev A A and Kim K W 2000 *Phys. Rev.* B **61** 13115
Pramanik S, Bandyopadhyay S and Cahay M 2003 *Phys. Rev.* B **68** 075313
Pershin Y V and Privman V 2004 *Phys. Rev.* B **69** 073310
[34] Pierret R F 2003 *Advanced Semiconductor Fundamentals* 116 (Englewood Cliffs, NJ: Prentice-Hall)
[35] Brand M A, Malinowski A, Karimov O Z, Marsden P A, Harley R T, Shields A J, Sanvitto D, Ritchie D A and Simmons M Y 2002 *Phys. Rev. Lett.* **89** 236601
[36] Pershin Y V 2005 *Physica* E **27** 77